Science of the Total Environment 512–513 (2015) 154–166

Contents lists available at ScienceDirect

Science of the Total Environment

journal homepage: www.elsevier.com/locate/scitotenv

Estimating the contribution of photochemical particle formation to ultrafine particle number averages in an urban atmosphere

N. Ma, W. Birmili *

Leibniz Institute for Tropospheric Research, Permoserstr. 15, 04318 Leipzig, Germany

HIGHLIGHTS

- A new method to determine source type contributions of ultrafine particles
- Identifying photochemical particle formation events
- Quantifying their contribution to annual average levels of ultrafine particles
- Discriminating particles from photochemical particle formation and traffic
- Photochemical particle formation events play a major role in the summer season
- The simplistic source apportionment helps exposure assessment

ARTICLE INFO

Article history:
Received 23 July 2014
Received in revised form 5 January 2015
Accepted 5 January 2015
Available online 21 January 2015

Editor: P. Kassomenos

Keywords:
Ultrafine aerosol
Aerosol particles
Particle number counts
Urban atmosphere
Photochemical particle formation
Traffic emissions
Differential mobility particle sizer
Health implications

ABSTRACT

Ultrafine particles (UFPs, diameter < 100 nm) have gained major attention in the environmental health discussion due to a number of suspected health effects. Observations of UFPs in urban air reveal the presence of several, time-dependent particle sources. In order to attribute measured UFP number concentrations to different source type contributions, we analyzed observations collected at a triplet of observation sites (roadside, urban background, rural) in the city of Leipzig, Germany. Photochemical new particle formation (NPF) events can be the overwhelming source of UFP particles on particular days, and were identified on the basis of characteristic patterns in the particle number size distribution data. A subsequent segmentation of the diurnal cycles of UFP concentration yielded a quantitative contribution of NPF events to daily, monthly, and annual mean values. At roadside, we obtained source contributions to the annual mean UFP number concentration (diameter range 5–100 nm) for photochemical NPF events (7%), local traffic (52%), diffuse urban sources (20%), and regional background (21%). The relative contribution of NPF events rises when moving away from roadside to the urban background and rural sites (14 and 30%, respectively). Their contribution also increases when considering only fresh UFPs (5–20 nm) (21% at the urban background site), and conversely decreases when considering UFPs at bigger sizes (20–100 nm) (8%). A seasonal analysis showed that NPF events have their greatest importance on UFP number concentration in the months May–August, accounting for roughly half of the fresh UFPs (5–20 nm) at the urban background location. The simplistic source apportionment presented here might serve to better characterize exposure to ambient UFPs in future epidemiological studies.

1. Introduction

Ultrafine particles (UFPs, Diameter < 100 nm) in urban air have gained attention due to a number of suspected health effects. Although contributing only little to particulate mass concentration, UFPs have considerable relevance for total particle number and surface. A main rationale for the health relevance of UFPs has been their small size, thus implying significant deposition in the deep lung and possible penetration through body tissue (HEI, 2013).

Since the late 1990s, a number of epidemiological studies indicated that human morbidity and mortality are affected by ambient UFP concentrations (e.g., Peters et al., 1997; Franck et al., 2011). At the time, this research was triggered by technical innovation, notably the ability to measure particle number size distributions and UFP number concentrations continuously. Nevertheless, the overall body of evidence for health effects of UFPs is still very limited in comparison to the many studies available for PM_{10} and $PM_{2.5}$ (Rückerl et al., 2011; HEI, 2013). UFPs are unlikely to become legally regulated in the very near future (WHO, 2013). According to these authoritative assessments, new epidemiological studies are desirable, which

* Corresponding author.

http://dx.doi.org/10.1016/j.scitotenv.2015.01.009

provide sound estimates of UFP exposure, and also include a source apportionment of UFPs.

The particular health-relevance of UFPs derives from the fact that combustion processes are a main source of UFPs in urban areas (Kumar et al., 2014). In cities around the world, much of ambient UFP exposure results from road traffic (Morawska et al., 2008).

High-temperature combustion in vehicular engines generates soot particles mainly bigger than 30 nm (Kittelson, 1998; Harris and Maricq, 2001), but also considerably smaller particles (Dp < 30 nm) when unburnt vapors nucleate in the cooling exhaust gas downstream (Giechaskiel et al., 2005). Diesel soot particles contain a solid core of elemental carbon coated with hydrocarbons of varying volatility. Exhaust gas nucleation particles, in contrast, are typically made of hydrocarbons and sulfate forming by nucleation during dilution and cooling of the exhaust. Although not consisting of a solid core, the latter may also contain carbon fragments and metallic ash. Various studies have reported on the chemical composition of particulate material emitted by diesel or gasoline engines (e.g., Graham, 2005; Maricq, 2007), although only few provided a specific chemical composition of ultrafine particles (e.g., Grose et al., 2006; Tobias et al., 2001; Sakurai et al., 2003). The tightening of emission standards during the past years has led to the development of engines that emit considerably less particle mass, while on the other hand, the emitted number of ultrafine particles may be even higher for some new engine techniques (Ntziachristos et al., 2004).

Many studies have attempted to characterize the temporal and spatial variability of ultrafine particles in urban areas (e.g., Costabile et al., 2009; Birmili et al., 2013). Evidently, the spatial variability of UFP concentrations depends on the spatial proximity to sources (Zhu et al., 2002) but also the dispersion conditions governed by topography, current wind speed and direction, and temperature inversions (Birmili et al., 2009a; Zwack et al., 2011).

However, there is another important source of particles that contributes significantly to UFP exposure in urban areas: secondary new particle formation. This gas-to-particle conversion process seems to happen almost everywhere in a continental atmosphere (Kulmala et al., 2004 and references therein). According to current research, photochemically produced sulphuric acid seems to be a necessary precursor for newly formed particles (Sipilä et al., 2010). Organic vapors might also participate in nucleation (Riccobono et al., 2014), and contribute much to the growth of nucleated particles. Relatively few studies have reported the chemical composition of these newly formed particles. Smith et al. (2005) found in the U.S. that ammonium sulfate accounted for the entire sampled mass of 6–15 nm particles after a nucleation event. They also found in Mexico that for 10–33 nm particles formed from nucleation, they contained far more organics, including nitrogen-containing organic compounds, organic acids, and hydroxy organic acids, than sulfates (Smith et al., 2008).

After nucleation, particles grow by condensation into bigger size ranges, eventually up to ~100 nm on the same day. Allan et al. (2006) showed that several hours after a nucleation event, the particles in nucleation mode were principally organic in composition. In the continental boundary layer, new particle formation events tend to happen simultaneously over areas of several 10 km, regardless whether the area is rural or urban (Vana et al., 2004; Wehner et al., 2007; Birmili et al., 2013).

This implies that in an urban area, there are several sources of UFPs, which are likely to differ in terms of chemical composition. It is currently unclear whether these different types of UFPs differ in their health effects or not. If the chemical composition is different between the ultrafine particles originating from vehicle exhaust and new particle formation, it can also be hypothesized that their health effects upon inhalation and long-term exposure are different as well. To better understand the health effects of urban ultrafine particles, it is desirable to discriminate at least the major source groups.

This paper attempts to isolate the fraction of UFP concentration in an urban area that originates from regional-scale secondary new particle formation events. Based on a one-year data set of aerosol number size distribution measured at roadside, urban background and regional background sites, two methods are applied to separae the contributions of UFPs originating from new particle formation and direct traffic-emission. The overall statistics and seasonal variations of the absolute and relative contributions of particles of different origins on the total number of ultrafine particles are analyzed and discussed in detail.

2. Experimental

2.1. Measurement sites

The data used in this study was collected at three observation sites in and around Leipzig, Germany: Leipzig-Mitte (L-Mitte, roadside), Leipzig-TROPOS (L-TROPOS, urban background), and Melpitz (regional background). The three sites are part of the German Ultrafine Aerosol Network (GUAN, Birmili et al., 2009b) and also participate in the TROPOS/Saxon State Office for Environment, Agriculture and Geology study of the effects of the introduction of the Leipzig Low Emission Zone (LEZ) on particulate air quality (Rasch et al., 2013).

The measurement site Leipzig-Mitte is located at roadside in the city center of Leipzig. The site borders the inner-city ring road, and is located in immediate vicinity to the central train station. Immediately north of the site, three main roads merge at an intersection with daily average traffic volumes around 4.4×10^4 vehicles (4.8×10^4 on workdays). Leipzig-Mitte experiences significant exposure to traffic-related pollutants, which is manifested by a traffic-related increment of 10 μg m^{-3} in PM_{10} mass concentration compared to an urban background location (Engler et al., 2012). The height of the aerosol inlet is 4.5 m.

Leipzig-TROPOS is situated on the roof of the TROPOS institute building, about 4 km distant from Leipzig-Mitte. Aerosol particles are sampled at a height of 16 m above the ground. Highly-trafficked roads touch the premises only at distances of 150 m and more. A comparison of the particle number size distribution at multiple sites in Leipzig confirmed Leipzig-TROPOS as a suitable urban background location (Costabile et al., 2009).

Melpitz is located 40 km northeast of Leipzig, and surrounded by flat and semi-natural grasslands without any obstacles in all directions. Agricultural pastures and wooded areas make up the wider regional surroundings. Besides GUAN, Melpitz contributes to WMO-GAW (Global Atmosphere Watch) as a regional background site. According to a pan-European comparison of tropospheric particle number size distributions, measurements at Melpitz can be taken representative for the rural atmospheric background in Central Europe (Asmi et al., 2011).

2.2. Instrumental

Particle number size distributions are recorded on a continuous basis using Twin Differential Mobility Particle Sizers (TDMPS). The three TDMPS instruments follow the basic set-up shown in Birmili et al. (1999), but are now upgraded with automatic sheath flow control and relative humidity (RH) control as described in Wiedensohler et al. (2012). Each instrument consists of two Differential Mobility Analysers (Vienna-type DMA), and two Condensation Particle Counters (CPC models 3772 and 3025A, TSI Inc., Shoreview, U.S.A.). Nafion membrane dryers were employed so that RH in the aerosol sample and sheath flows was always kept below 40%. The TDMPS nominally scans across a particle size range 3–800 nm. Due to enhanced measurement uncertainties below 5 nm, however, only the diameter range 5–800 nm was subsequently used. The time resolution of the measurement in Leipzig-Mitte is 10 min, while it is only 20 min for Leipzig-TROPOS and Melpitz due to the presence of an additional thermodenuder. Quality assurance of the measurements involves monthly checks of the particle sizing (PLS spheres), and an annual comparison against a reference Mobility Particle Size Spectrometer

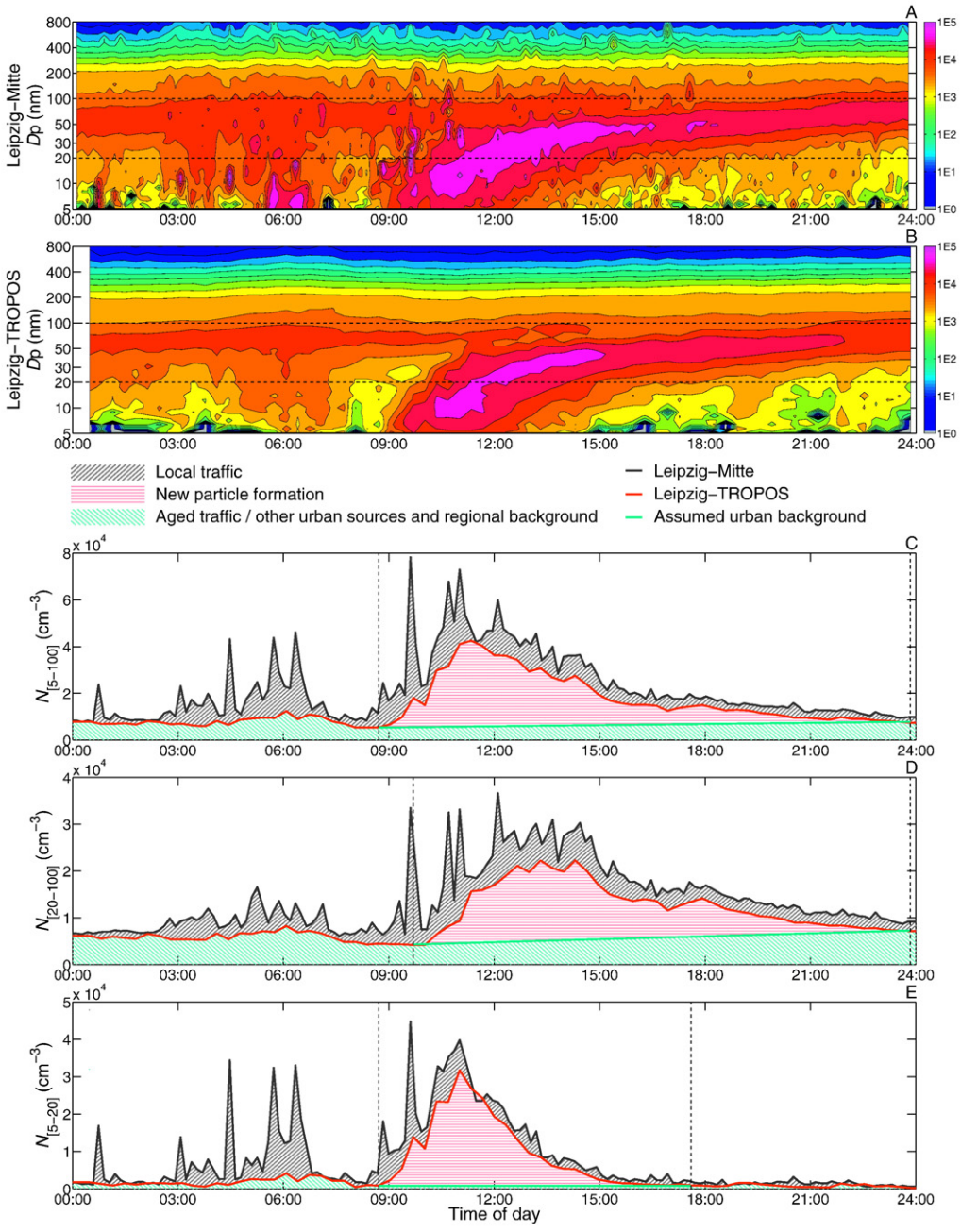

Fig. 1. Estimating the contribution of a photochemical particle formation event on ultrafine particle number concentration in Leipzig, Germany with the simple chord method "A". The diagrams show exemplary data from July 24, 2012. The sub-figures A) and B) show contour diagrams of the particle number size distribution ($dN/d\log D_p$ in cm^{-3}) at roadside (Leipzig-Mitte) and in the urban background (Leipzig-TROPOS), respectively. The sub-figures C)–E) show time series of ultrafine particle number concentration $N_{[5–100]}$, $N_{[20–100]}$ and $N_{[5–20]}$, corresponding to the size intervals 5–100 nm, 20–100 nm and 5–20 nm, respectively. The sub-figures C)–E) illustrate the split of measured concentrations into the various source contributions "urban background" (without new particle formation), "new particle formation", and the additional traffic contribution seen at roadside.

on site. This reference instrument is, in turn, checked frequently in the calibration laboratory against total particle counters (CPCs) that serve as a reference for particle number concentration. Particle mobility distributions were inverted using a multiple-charge inversion algorithm (Pfeifer et al., 2014), with subsequent corrections applied to account for the counting efficiency of the CPC, the transfer function of the DMA, and diffusion losses in aerosol dryers and connecting tubes (Wiedensohler et al., 2012). The relative inter-comparability of number concentrations at a specific size bin is assumed to be 10% at 20 nm, and 20% at 5 nm. Black carbon data were measured at all stations for the PM_{10} range by multi angle absorption photometers (MAAP) using a mass absorption coefficient of 6.6 g m^{-2}.

2.3. Detection of new particle formation events

The number size distributions of photochemically induced particle bursts observed at a stationary site show, in fully developed version, a number of recurring characteristics. Fig. 1A and B illustrates such a particle formation burst occurring simultaneously at the two observation sites L-TROPOS and L-Mitte. The burst can be detected by high particle number concentrations around midday, followed by a subsequent, gradual shift of the new nucleation mode towards bigger diameters.

There have been several suggestions in the literature to identify such new particle formation (NPF) events from extended data sets: Dal Maso

et al. (2005) formalized, on the basis of data from the regional background site Hyytiälä in Finland, a decision path involving the number concentration of nucleation mode particles, the persistence of that mode, changes with respect to geometric mean diameter, and the occurrence of fluctuations in the mode's number concentration. Their scheme provides four possible categories for an observation day, including two NPF event types, a non-event, and an undefined category. Alternative approaches have included a detection based on the number concentration of the smallest particles alone (Birmili et al., 2003), or the similarity of the diurnal data with a pre-defined set of particle formation events based on multiple moments of the particle number size distribution (Heintzenberg et al., 2007). All studies have in common that they consider time series of particle number concentration with a defined upper cut-off that distinguishes the newly formed particles from those already present at bigger sizes.

The method used in this paper is a simplified variant of Dal Maso's procedure (Dal Maso et al., 2005). Particle number size distributions were visually inspected for the sites Leipzig-TROPOS and Melpitz, determining the occurrence of NPF events at both sites independently. The requirements for a day to qualify as a NPF event were: 1) a substantial increase in the number concentration of particles <20 nm ($N_{[5–20]}$) during the time window 09:00–15:00 LT, 2) $N_{[5–20]}$ being significantly elevated above the nocturnal background, 3) the burst having a minimum duration of 1 h, and 4) a decrease in $N_{[5–20]}$ towards the end of the day. The observation of a gradual increase in nucleation mode diameter was not a necessary criterion to qualify as a NPF day, but was nevertheless visible in most cases.

2.4. Isolating the contribution of particle formation bursts

2.4.1. General concept

To split observed UFP number concentrations into different source type contributions, we assume that the concentrations at the urban background site ($N_{\text{L-TROPOS}}$) can be expressed, at any time, as a superposition of particles labeled "urban background" (N_{UBG}) and particles originating from new particle formation bursts (N_{NPF}).

$$N_{\text{L-TROPOS}} = N_{\text{UBG}} + N_{\text{NPF}} \quad (1)$$

"Urban background" particles are those present in urban atmosphere in the absence of a particle formation event, and contain particles from the regional background, and such originating from traffic and other urban sources dispersed across the city.

Fig. 1C–E illustrates the evolution of $N_{\text{L-TROPOS}}$ on an exemplary day, July 24, 2012: Between 00:00 and 07:00 LT, a rather steady level of $N_{[5–100]}$ and $N_{[20–100]}$ can be seen at Leipzig-TROPOS (red line). Between 07:00 and 09:00 LT these values decrease as a consequence of vertical mixing and the expansion of the urban boundary layer. The result is a notable concentration minimum, most prominent for particles <20 nm at Leipzig-TROPOS in the contour diagram of Fig. 1B. At 09:00 LT, the photochemical particle burst occurs, drastically raising the concentrations $N_{[5–100]}$ and $N_{[5–20]}$ until they reach their peak value at Leipzig-TROPOS at 11:30 LT. After new particle formation ceased, the nucleation mode particles visibly grow in diameter by processes such as condensation and coagulation. The number concentrations $N_{[5–100]}$ and $N_{[5–20]}$ ($N_{[20–100]}$ to a lesser degree), however, decrease during the following hours, returning the concentrations to levels close to their initial night-time level.

To numerically extract the contribution of NPF events, we developed two methods, which differ in the approach how urban background concentrations would evolve in the absence of a NPF event.

2.4.2. Method A: The simple chord method

The concept of method A is to divide the integral under the time series of particle number concentration at the urban background site (Leipzig-TROPOS) into two areas by placing a straight chord. The chord is designed to approximate the evolution of $N_{\text{L-TROPOS}}$ in the absence of NPF, attributing the integral section above the chord to the NPF event. The area below the chord, also including concentrations outside the time of the NPF burst is considered the urban background concentration without the effect of NPF. The chord is made to start in the concentration minimum prior to the NPF event. This is the time when the urban atmosphere is assumed to be well-mixed already, but when particles from the nucleation burst have not appeared yet. The end of the chord was attached to the concentration value of $N_{\text{L-TROPOS}}$ at 24:00 LT unless the NPF event was interrupted by incidents such as an air mass change.

Once the position of the chord had been fixed, we computed the daily average number concentration due to photochemically formed particles ($\overline{N}_{\text{NPF}}$) for the three particle size ranges integrating the red shaded areas above the chord displayed in Fig. 1A–C. Details of the calculation are supplied in Appendix A.

Two issues of the method are addressed here that might influence the results with respect to $\overline{N}_{\text{NPF}}$. These concern first, the terminus point of the chord and second, the appropriateness of a straight chord line.

For most NPF bursts, we could confirm that at 24:00 LT the concentrations levels had returned close to their initial background (91% for $N_{[5–20]}$ and 72% for $N_{[20–100]}$). In cases when particles from the NPF burst are still visibly present at 24:00 LT, the use of the method will cause an underestimation of the number of particles being attributable to the NPF event. Therefore, two alternative options to terminate the chord line were explored, being discussed in detail in the uncertainty analysis in Section 4.

A critical assumption of method A is that N_{UBG} would have evolved in the same linear fashion as the linear chord in the presence of the NPF event. While the concept of a simple straight chord was motivated by the typical behavior of $N_{\text{L-TROPOS}}$ on non-event days, it might not be appropriate for all cases. As a consequence, we improved on this aspect, which led to the development of method B described in the following section. The uncertainty of method A in comparison with method B will be discussed in Section 4.1.

2.4.3. Method B: Using diurnal patterns on non-event days

Method B was conceived to overcome the somewhat arbitrary use of a straight chord to approximate the diurnal cycle of UFPs in the urban background atmosphere in the presence of the NPF event. Hence, it was a critical question which portions of the data should be selected to approximate the true behavior of N_{UBG}?

Statistical studies of regional NPF events highlighted their connection to days with intense solar irradiance (e.g., Boy and Kulmala, 2002; Birmili et al., 2003). In meteorological terms, solar irradiance causes convection, turbulence, and a well-mixed boundary layer. In an urban atmosphere, such convection and mixing greatly affects pollutant dispersal. This implies that for the estimation of N_{UBG}, data from such well-mixed meteorological situations should be preferred.

Fig. 2 displays the daily averaged global radiation measured in 2012, showing similar observation patterns in Leipzig and Melpitz. As can be seen, NPF events occur almost exclusively on days with a daily average radiation of more than 100 W m^{-2}, but there are also a considerable number of days with high solar radiation and no NPF events. Our approach was to estimate N_{UBG} from the diurnal cycles of $N_{\text{L-TROPOS}}$ on these non-events with high global radiation.

As a basis for the non-NPF days, we selected days with a global mean radiation of more than 100 W m^{-2}. Above this threshold, non-NPF days amount to a similar number as NPF event days and thus represent a statistically comparable population.

Fig. 3 shows annual averages of UFP number concentrations for the three number metrics and the three observation sites. The display now distinguishes between NPF event days, non-NPF days with high global radiation (daily average > 100 W m^{-2}) and non-NPF days with

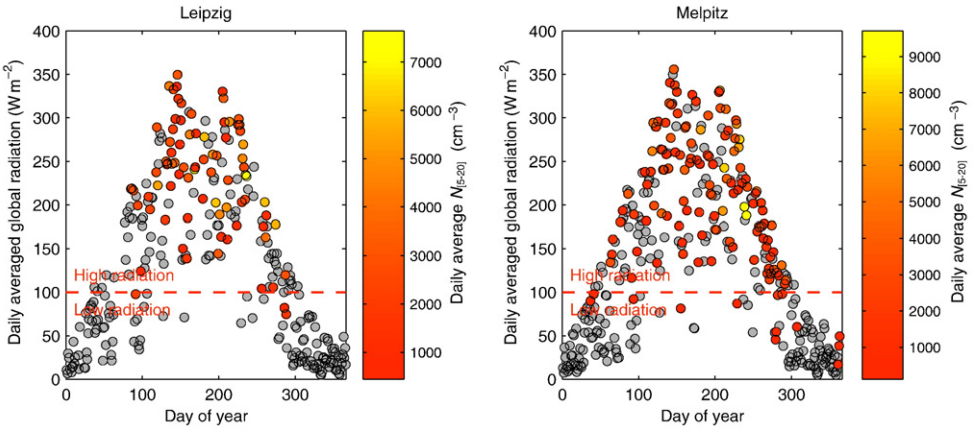

Fig. 2. Daily average global radiation measured in Leipzig (left) and Melpitz (right), measured with pyranometers. Days with new particle formation events are marked in color, encoding the daily average of $N_{[5–20]}$ (in cm^{-3}). The dashed line was chosen to discern non-NPF days with "high" and "low" radiation, respectively.

low global radiation. It can be seen that the diurnal cycles on $N_{L\text{-}TROPOS}$ for NPF event days (red) and non-NPF days with high global radiation (green) agree rather closely until 09:00 LT and after 21:00 LT. This supports the hypothesis that the diurnal cycles on non-NPF days with high global radiation can be used as a surrogate for N_{UBG}.

It can be seen that in comparison to the simple straight chord used in method A, UFP number concentration tends to further drop after 09:00 LT before reaching the daily average minimum around 15:00 LT. The contribution of new particle formation can be calculated as numerical integration of the red shade area, taking into account of the number of new particle formation event days. For details of the calculation, see Appendix B.

For completeness, Fig. 3 also displays diurnal cycles of N for low-radiation non-NPF days as green dashed lines. It can be seen that these are notably different from the cycles of high-radiation non-NPF days, very likely due to the different meteorological conditions, and also compare less well with the data on NPF event days outside the NPF period. This confirms that it is necessary to distinguish different periods according to the intensity of solar irradiation.

A drawback of method B, in comparison with method A, is that it can currently only be applied for average data, because it is necessary to perform differences between data averaged for certain groups of days (high radiation/low radiation). Moreover, the results might be influenced, for example, by the choice of the radiation threshold in Fig. 2. These uncertainties will be addressed as part of an uncertainty discussion in Section 4.

2.5. Separating the contributions of regional background, local traffic, and aged traffic/other urban sources

Having concentrated on measurements at the urban background site (Leipzig-TROPOS) up to this point, we now extend the picture by considering roadside (Leipzig-Mitte) and regional background measurements (Melpitz). As mentioned above, "urban background" particles (N_{UBG}) is perceived to be a superposition of regional background aerosol (N_{RBG}), and aerosol originating from within the city ($N_{AT\&OS}$).

$$N_{UBG} = N_{RBG} + N_{AT\&OS} \quad (2)$$

$N_{AT\&OS}$ denotes "aged traffic & other sources" particles, in contrast to the "fresh" traffic particles at roadside discussed later. The urban particles are thought to stem from the various diffuse sources situated upwind the measurement site (but within the city), and involve sources from traffic, industry, domestic heating, etc. "Regional background"

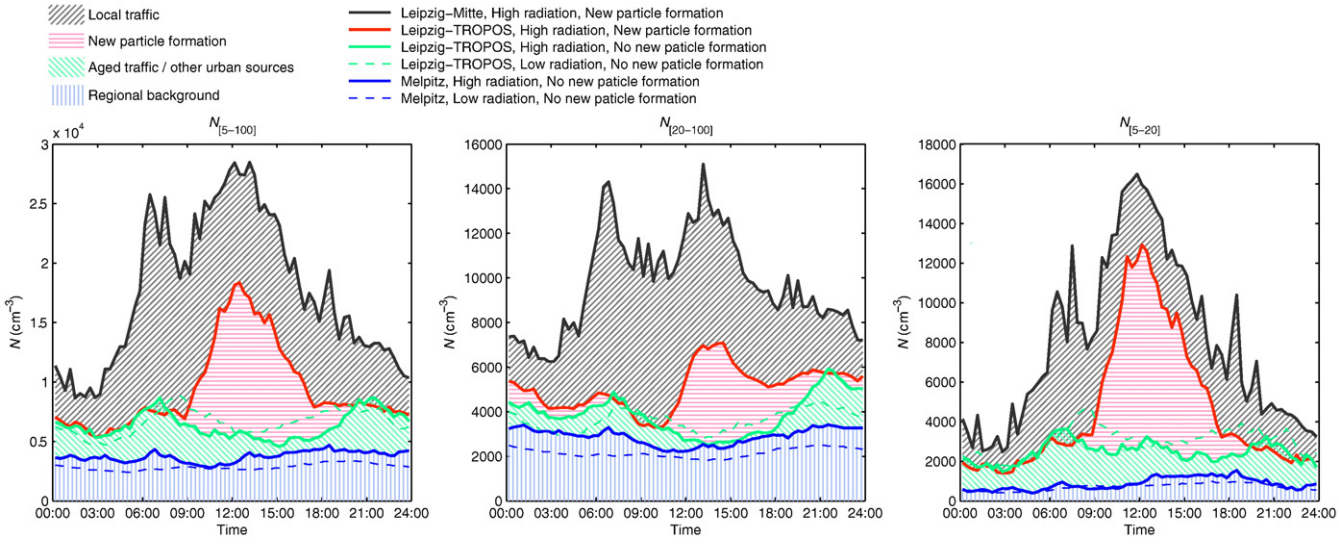

Fig. 3. Estimating the contribution of a photochemical particle formation event on ultrafine particle number concentration in Leipzig, Germany with method B. The diagrams show the average diurnal patter of N measure at roadside (Leipzig-Mitte), urban background (Leipzig-TROPOS) and regional background (Melpitz) for high/low radiation NPF/non-NPF days.

particles likely stem from rather similar sources in different cities much further upwind, and can even include photochemically formed particles if this formation took place the day before or earlier. An obvious separation criterion is particle age.

N_{RBG} is estimated from the measurement at the regional background (Melpitz). One needs the assumption that Leipzig and Melpitz are in the same overall air mass, which is warranted for the overwhelming number of cases in view of the spatial proximity of 40 km.

Taking into account the additional NPF term, a number concentration of UFP measured at the urban background site ($N_{L\text{-}TROPOS}$) can be written as:

$$N_{L-TROPOS} = N_{RBG} + N_{AT\&OS} + N_{NPF}. \quad (3)$$

At the roadside site, we assume that UFP concentrations ($N_{L\text{-}Mitte}$) comprise an additional fourth particle type, such emitted from local motor vehicles (N_{LT}):

$$N_{L-Mitte} = N_{RBG} + N_{AT\&OS} + N_{NPF} + N_{LT} \quad (4)$$

The paradigms given in Eqs. (2) and (4) were suggested by Lenschow et al. (2001) for urban PM_{10} mass concentrations, and correspond to a linear additive model for urban pollutant particle concentrations The Figs. 1C–E and 3 suggest that this principle is sound for our configuration of observation sites in that the measurement at Leipzig-TROPOS serves as a lower envelope for the measurement at Leipzig-Mitte. In correspondence with the short distance of 4 km between the two urban sites, the Lenschow paradigm appears to be justified. A subtraction of $N_{L\text{-}TROPOS}$ from $N_{L\text{-}Mitte}$ will then yield an approximation of the local traffic-induced component N_{LT} at Leipzig-Mitte.

When isolating the contribution of NPF events (N_{NPF}), another assumption is needed, notably regarding the spatial homogeneity of these events. At traffic-related sites such as Leipzig-Mitte, the diurnal cycle of N can be of such complicated shape that it seems impossible to extract N_{NPF} from the data there (Fig. 1). Instead, we need to rely on urban background data for the determination of N_{NPF}, and generalize this value on roadside conditions.

Studies of NPF events involving multiple observation sites in Europe have suggested that NPF events can be a meso-scale phenomenon that happens simultaneously over large spatial areas. While Vana et al. (2004) report a maximum spatial extent of "more than 1000 km" during their study in Finland and Estonia, typical spatial extents of several 10 to 100 km have been suggested for Central Europe based on multiple site observations (Wehner et al., 2007; Costabile et al., 2009; Birmili et al., 2013). For the city of Barcelona, Spain, three different types of nucleation events have been identified, depending on their coincidence in the urban and regional environment (Dall'Osto et al., 2013). The Central European studies correspond with our own observations that NPF bursts coincide to very high coincidence within the area of Leipzig, though to a lesser extent with the Melpitz, distant at 40 km.

In analogy to Leipzig-TROPOS, UFP concentrations in the regional reference site Melpitz are assumed to consist of a regional background component N_{RBG}, and the newly formed aerosol N_{NPF}:

$$N_{Melpitz} = N_{RBG} + N_{NPF}. \quad (5)$$

Detailed information on the calculation of the contributions of regional background, local traffic, and aged traffic/other urban sources with the two methods is shown in Appendices A and B.

3. Results

3.1. Overview of ultrafine particles concentration

Atmospheric particle number size distributions (5–800 nm) were analyzed for the whole year 2012. For the urban sites Leipzig-TROPOS and Leipzig-Mitte, only such days were considered when data was available for both sites. After quality control, 308 days of measurement were usable for Leipzig-TROPOS and Leipzig-Mitte, of which 283 days were without missing data and 25 days were with sufficient data (more than 60%) to evaluate the parameters described in Section 2.3. For Melpitz, 356 days of measurement were usable, of which 330 days were without missing data and 26 days with sufficient data to determine the integral parameters.

In Leipzig-TROPOS and Leipzig-Mitte, new particle formation events occurred on 109 days, accounting for 35% of the total valid days. The daily maximum in $N_{[5-100]}$ amounted to more than 3×10^4 cm^{-3} on 42 days and to more than 5×10^4 cm^{-3} on 8 days in both sites. In the station of Melpitz, NPF events happened on 160 days, accounting for 45% of the total 356 valid days. The daily maximum $N_{[5-100]}$ is more than 3×10^4 cm^{-3} on 43 days and is more than 5×10^4 cm^{-3} on 13 days. It is worth to note that the frequency of new particle formation events was higher in Melpitz than in Leipzig. In contrast to the close pair of urban sites Leipzig-Mitte/Leipzig-TROPOS, NPF events at Melpitz coincided to a lesser degree with those in the city. We assume that the 40 km distance between Melpitz and Leipzig-TROPOS, compared to a 4 km distance between Leipzig-Mitte and Leipzig-TROPOS, plays a role for this spatial heterogeneity. Although by far most NPF events occurred simultaneously at all three sites, exceptions occurred, and the absolute concentration of newly formed particles in Leipzig were not necessarily the same at Melpitz.

We scrutinized possible reasons for this. According to the global radiation measurements, solar irradiance in Melpitz exceeded that in Leipzig by 2.9%. This difference is close to the instrumental uncertainties and therefore insufficient to explain the different frequency of NPF events. It is our impression that the low background concentration of $N_{[5-20]}$ at Melpitz makes NPF events there easier to detect visually: In the time window 06:00–12:00, Melpitz background $N_{[5-20]}$ amounts to only one third of the values measured at Leipzig-TROPOS only (Fig. 3). The weakest NPF events at Melpitz show peak values of $N_{[5-20]}$ around 3.00×10^3 cm^{-3}, i.e., close to the average concentration at Leipzig-TROPOS on non-events (3.02×10^3 cm^{-3}). We therefore assume that the different background number concentration levels are one reason for the disagreement of the NPF event frequencies at Melpitz and Leipzig-TROPOS. An analysis of the condensation sink parameter (calculated for dry conditions; not shown) proved to be inconclusive, the values at Melpitz being slightly lower compared to Leipzig-TROPOS. Other reasons, which are harder to verify, might be related to differences in the evolution of the boundary layer height and/or differences in ozone precursors.

Table 1 lists the statistics of the number concentration of UFPs in different size ranges at three sites. We opted for three particle metrics involving the size ranges 5–20 nm, 5–100 nm, and 20–100 nm. These intervals were motivated by the lower size cut of our instrumentation (5 nm), an upper cut-off diameter which provided useful for the detection of photochemical particle formation bursts (20 nm), and the definition of ultrafine particles (100 nm). The annual mean values are usually sorted well along the order roadside (Leipzig-Mitte) > urban background (Leipzig-TROPOS) > regional background (Melpitz). $N_{[5-100]}$ at roadside is about twice that of the values in the urban background, indicating that traffic-emitted particles contribute half of the total number of ultrafine particles at roadside. $N_{[5-100]}$ in the urban background is 56% higher than in the regional background, indicating a presence of UFPs due to urban sources. The number concentrations are also differentiated according to NPF event days and non-event days, and highlight the relevance of this process for the UFP number budget.

Table 1
Statistics of UFP number concentration (in 10^3 cm^{-3}) in Leipzig for the three concentration metrics $N_{[5–100]}$, $N_{[20–100]}$ and $N_{[5–20]}$, corresponding to the particle size intervals 5–100 nm, 20–100 nm and 5–20 nm, respectively. UFP number concentrations are provided for the three observation sites Leipzig-Mitte (roadside), Leipzig-TROPOS (urban background), and Melpitz (regional background). These statistics are based on daily average values.

	$N_{[5–100]}$			$N_{[20–100]}$			$N_{[5–20]}$		
	Roadside	Urban bg.	Regional bg.	Roadside	Urban bg.	Regional bg.	Roadside	Urban bg.	Regional bg.
Mean	15.8	7.58	4.86	8.79	4.05	3.14	7.02	3.53	1.72
Std. Dev.	5.64	3.10	3.12	2.98	1.80	1.69	3.18	1.97	1.73
Median	15.5	7.01	3.85	8.53	3.81	2.76	6.58	3.07	1.11
Mean on NPF days	17.8	9.38	6.97	9.76	4.81	4.07	8.04	4.58	2.90
Mean on non-NPF days	14.8	6.71	3.16	8.28	3.69	2.37	6.48	3.02	0.753
Max.	50.7	20.3	22.0	19.6	12.2	11.2	33.4	12.2	10.8
Min.	5.22	1.41	0.865	2.44	0.897	0.720	1.16	0.353	0.0813

3.2. Absolute and relative contributions of origination groups

Fig. 4 displays the estimates of the UFP source type contributions derived by the two methods A and B introduced in in Section 2.4, providing annual averages over all NPF event days and non-event days. A first observation is that both methods yield rather similar results. (We will usually discuss the values obtained by method A and add the results of method B in brackets.).

For the urban background site Leipzig-TROPOS, 14.0% (14.1%) of annual average $N_{[5–100]}$ was attributable to NPF events, and 47.5% (43.8%) to the regional background. The remainder of 38.5% (42.1%) was attributed to the category "aged traffic & other sources". The roadside concentrations (Leipzig-Mitte) are assumed to be split so that local traffic adds on top of the concentrations measured in the urban background (cf. Section 2.5). While the absolute contributions of NPF events, regional background and aged traffic/other urban sources remain the same, their relative contributions decrease to 6.74% (6.79%), 22.8% (21.1%) and 18.5% (20.3%), respectively, with freshly emitted traffic particles accounting for 51.9% (51.8%) of $N_{[5–100]}$. At rural Melpitz, the average estimate of particles originating from NPF events is 1.25×10^3 cm^{-3} (1.46×10^3 cm^{-3}), which slightly exceeds those in the city. As the regional background concentrations are significantly lower than in the city, particles due to NPF events account for 26.0% (30.3%) of in $N_{[5–100]}$, nearly twice as much as in Leipzig-TROPOS.

When comparing the different metrics, it is a somewhat intuitive result that the relative contribution of NPF descends from $N_{[5–20]}$ to

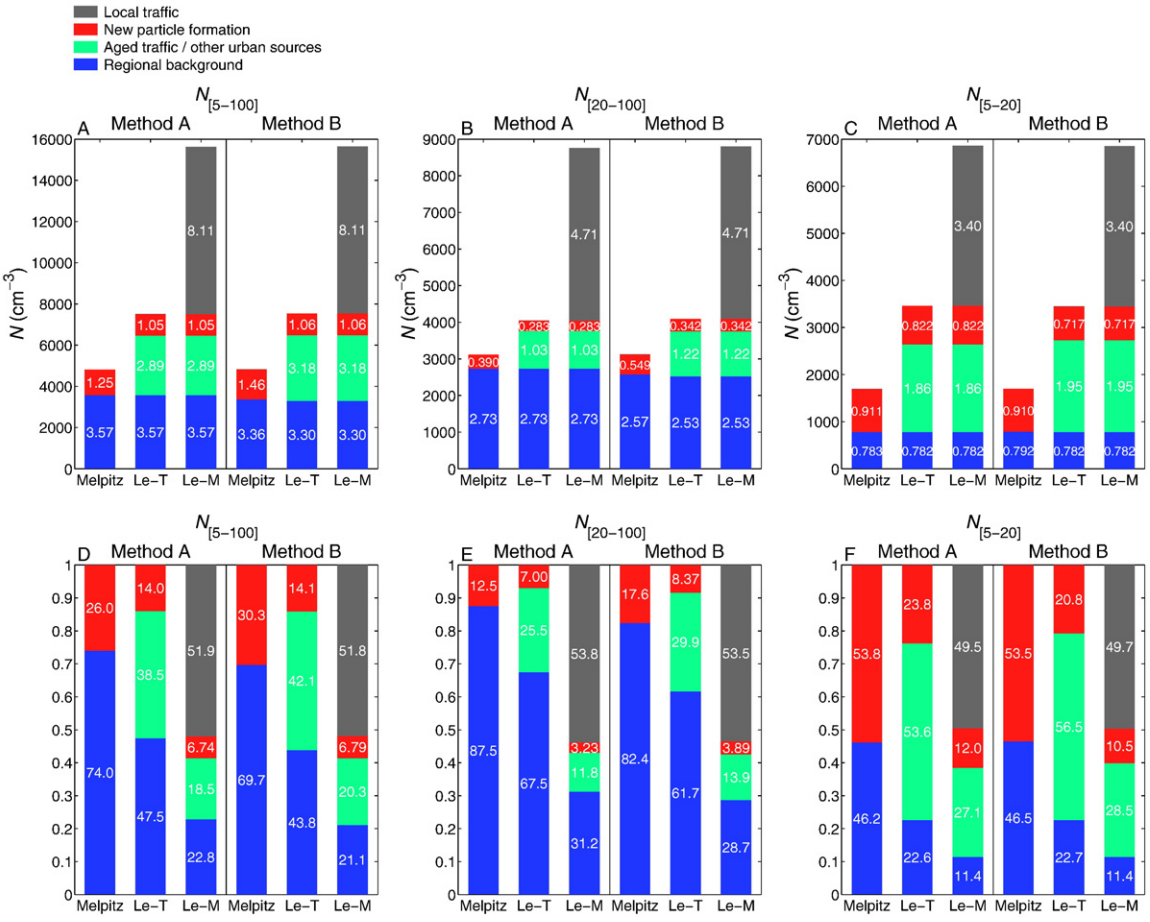

Fig. 4. Split of the 2012 annual mean value of ultrafine particle number concentration in Leipzig, Germany, into specific source type contributions. The upper diagrams A)–C) show the absolute concentrations of $N_{[5–100]}$, $N_{[20–100]}$ and $N_{[5–20]}$ in 10^3 cm^{-3} while the lower diagrams D)–F) illustrate the relative contributions. Contributions were estimated for a regional background site (Melpitz), an urban background site (Leipzig-TROPOS), and an urban roadside site (Leipzig-Mitte) featuring a nearby traffic volume of ca. 4.8×10^4 veh/day.

$N_{[5-100]}$ and further to $N_{[20-100]}$. The metrics starting at 5 nm capture the full impact of NPF events on particle number concentration, albeit particles in the range below 20 nm tend to rapidly disappear towards the end of the day as a result of coagulation and condensation. Although a well-known fact, Fig. 4 highlights the relevance of the choice of a particular particle size range when reporting total particle number concentrations.

The highest contribution of particles originating from NPF events, 53.8% (53.5%), was determined for the rural Melpitz site and the metric $N_{[5-20]}$. This is straightforward to understand in view of the relatively low background of directly emitted anthropogenic UFPs in the rural region. It is interesting to note that regardless of the choice of the metric, the contribution of traffic to the concentrations at roadside (Leipzig-Mitte) remains roughly constant at 50%. This suggests that traffic-derived particles contribute in similar proportions to the nucleation mode size range (5–20 nm) and the Aitken mode size range (20–100 nm).

Naturally, there is great variability in the concentration of NPF events to number concentration on a day-to-day basis. At Leipzig-Mitte, for example, the relative contribution of traffic-derived particles exceeds 50% on 59% of all days, with the overall maximum being 84%. At the urban background site Leipzig-TROPOS, the relative contribution of NPF events exceeded 50% on 46% of the NPF days for $N_{[5-20]}$, with a maximum of 85%. At rural Melpitz, these figures are naturally higher, the relative contribution of NPF events exceeding 50% on more than two thirds of the NPF days (70%), and a maximum contribution on a single day being 96%.

3.3. Seasonal effects

As suggested in several previous works (Dal Maso et al., 2005; Manninen et al., 2010; Hamed et al., 2010), photochemical particle formation bursts exhibit significant seasonal variation. Most previous studies forward the seasonal cycle of solar radiation, the availability of biogenic organic precursors, as well as the seasonal cycle of the mixed layer height as reasons for this behavior. As a consequence, we opted to calculate the relative source type contributions for each month in 2012 individually. Because method B needs long-term averages for the calculations, only the results derived with method A are shown here.

It can be seen in Fig. 5 that the relative contribution of particles due to NPF events shows a pronounced seasonal pattern both in Leipzig and Melpitz. The peak of the monthly relative contribution is around June and July. Virtually no NPF events occurred between November and February. While similar seasonal patterns have been found in many other European boundary layer sites, an opposite behavior, with high frequency in winter and low frequency in summer has also been found in certain locations (e.g., Birmili et al., 2003; Shen et al., 2011).

In the urban background site (Leipzig-TROPOS) the relative contribution of NPF events peaks in June for $N_{[5-100]}$ (31.6%) and in August for $N_{[5-20\ nm]}$ (50.9%). The monthly relative contribution of regional background particles does not change much in different months. It is perhaps interesting that although photochemical particle production contributes significantly to total number in summer and less in winter, no comparable pattern can be seen in absolute number concentrations $N_{[5-100]}$, $N_{[20-100]}$ and $N_{[5-20]}$. A main argument is that in the cold season, atmospheric mixing tends to be limited, thus enhancing the near-surface concentrations of anthropogenic particles. In addition, anthropogenic emissions are higher in winter due to sources such as domestic heating, which can be found as responsible for the increase of the relative contribution of aged traffic/other urban sources in the cold season. These two processes apparently counterbalance with respect to the overall annual cycle of total particle number concentration.

At roadside, the maximum monthly relative contribution of NPF events is 18.3% (August) for $N_{[5-100]}$ and 32.9% (August) for $N_{[5-20]}$. The monthly relative contribution of local traffic and regional background

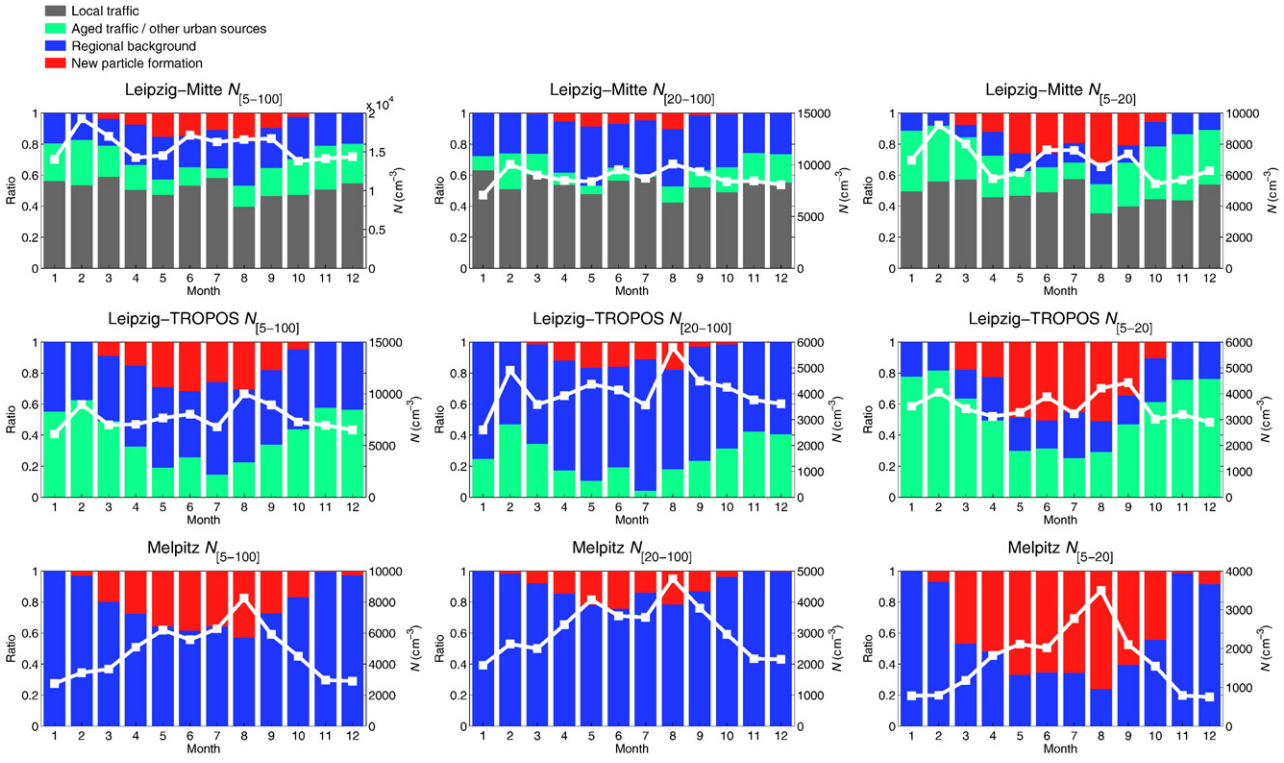

Fig. 5. Monthly split of ultrafine particle number concentration in Leipzig, Germany, into relative source type contributions. The diagram matrix distinguishes between estimates for the roadside site Leipzig-Mitte (top row), the urban background site Leipzig-TROPOS (middle row), the regional background site Melpitz (bottom row), and the particle number metrics $N_{[5-100]}$, $N_{[20-100]}$ and $N_{[5-20]}$ (from left to right). Each sub-figure contains, as an overlay, a monthly time series of absolute ultrafine particle number.

particles does not change much in different months. For all the three size ranges shown here, the monthly relative contribution is around 50%, as stated Section 3.2.

In the rural site Melpitz, due to the absence of direct traffic emissions and a lower level of background aerosol, the newly formed particles show a higher overall contribution in most of the months. The maximum monthly relative contribution of newly formed particles is 42.8% (August) for $N_{[5–100]}$ and is even up to 75.9% (August) for $N_{[5–20]}$. With less influence from local anthropogenic emissions, UFP number concentrations are dominated mainly by NPF events at Melpitz. The total number concentrations $N_{[5–100]}$, $N_{[20–100]}$ and $N_{[5–20]}$ show evident seasonal pattern, with high values in warm season and low values in cold season.

4. Uncertainties

This section recapitulates some methodological uncertainties related to the two methods A and B introduced in Section 2.4. Although the basic idea behind the two methods is similar, systematic and accidental differences are expected.

4.1. Divergence between methods A and B for the average case

There are several uncertainties expected with the use of method A (Section 2.4.2). In particular, the method may underestimate the contribution of photochemically formed aerosol, since the actual level of background aerosol might be lower than suggested by the straight chord due to atmospheric dilution of pollution aerosol in the afternoon (Fig. 3). To estimate a typical bias, method A is applied on the average diurnal pattern shown in Fig. 3, yielding the following values of N_{NPF}: 2.13×10^3 cm^{-3} (size range 5–20 nm), 2.47×10^3 cm^{-3} (5–100 nm), and 6.72×10^2 cm^{-3} (20–100 nm). These compare to the following values obtained from method B: 2.09×10^3 cm^{-3} (5–20 nm), 3.05×10^3 cm^{-3} (5–100 nm), and 1.23×10^3 cm^{-3} (20–100 nm). Thus, for the single case in Fig. 3 method A underestimates N_{NPF} about 20% for the diameter range 5–100 nm and by 45% for the range 20–100 nm. An obvious reason for the divergence is that the (non-photochemical) background number concentration, especially in the case of $N_{[5–100]}$ and $N_{[20–100]}$, further decreases throughout the afternoon, and does not follow a straight line.

When looking at the statistical results in Fig. 4, however, the methodological differences appear much smaller. The actual reason is that many NPF events last just a few hours, unlike the average behavior depicted in Fig. 3. In the case of short NPF events, the straight chords of method A are closer to the background level, resulting in a better agreement of the methods.

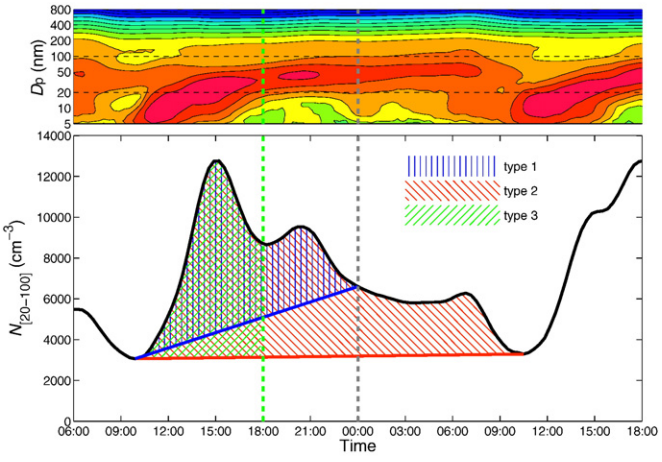

Fig. 6. Illustrating the effect of different chord positions on the amount of particle number concentration attributable to NPF. Exemplary data from Leipzig-TROPOS (August 14, 2012). For better illustration, the time series have been smoothed.

4.2. Sensitivity study of three variants of method A

Another issue is that in some cases, the nucleation mode generated by NPF remains in the local atmosphere until the following day, i.e., past 24:00 LT. This will also cause an underestimation of the contribution of new particle formation since those remnants will automatically be classified as background particles on the subsequent day. An additional issue is that particles emitted from local traffic past 18:00 LT may interfere with the signal caused by NPF and thus be mis-classified as a contribution by NPF. As the surviving nucleation mode particles will mostly grow beyond 20 nm in size, the underestimation will mainly affect $N_{[20–100]}$.

To estimate typical biases induced by these two issues, method A was modified into two additional variants and applied to the entire data set. Fig. 6 schematically describes the modification of method A based on the smoothed time series of $N_{[20–100]}$ on August 14 and 15, 2012. In this concrete case, the NPF particles remain until the morning of the next day while the influence of traffic can also been seen in the evening and the morning of the next day. The blue-shaded area is the contribution of NPF derived with original method A (named "type 1"). It is clear that the contribution of the remaining NPF particles on the next day is ignored, and the level of urban background aerosol might be overestimated. For a modified method A "type 2", shown as a red shade in Fig. 6, the chord is terminated at the low point of N on the subsequent morning, i.e., not necessarily limited to 24:00 LT of the same day. The level of urban background aerosol defined by this method appears more reasonable than type 1 (original method A), although the particles emitted by traffic in the evening always tend to be counted into the contribution of NPF as well. The modified method A "type 3", shown as a green shade in Fig. 6 avoid the influence of traffic, generally cutting off any contributions after 18:00 LT on the day of NPF.

Alike method A "type1", the variants "type 2" and "type 3" were applied to the entire 2012 data set. Table 2 shows the absolute and relative contributions (in brackets) of NPF with regard to the annual average of $N_{[5–100]}$, $N_{[20–100]}$ and $N_{[5–20]}$. Not unexpectedly, the highest contribution was given by the sub-method type 2, while the lowest contribution was given by sub-method type 3. For $N_{[5–20]}$, there is virtually no difference between the three sub-methods; the explanation is that $N_{[5–20]}$ almost always decreases to very low background levels before 24:00 LT. For $N_{[20–100]}$, in contrast, the results differ most. Counting any evening traffic particles as NPF contribution, the contribution yielded by sub-method type 2 is 30% higher than that of original method A. Excluding any possible influence of traffic in the evening, sub-method type 3 yields the lowest value of N_{NPF}, although the difference to the original method A is only 14%.

It should be emphasized that the event depicted in Fig. 6 is not necessarily the regular case. Most NPF events terminate before 24:00 LT, with many being interrupted or terminated before 18:00 LT. Therefore, the differences reported in Table 2 appear more moderate than anticipated from Fig. 6. We consider the sub-methods type 2 and type 3 to provide the following uncertainties for method A with respect to the terminal point of the chord: ~2% for $N_{[5–20]}$, ~7% for $N_{[5–100]}$, and ~25% for $N_{[20–100]}$.

4.3. Overall assessment of method B

Method B makes use of average diurnal cycles of N on NPF event days and non-NPF days. We conducted a sensitivity analysis whether the results might be influenced by the selection of the threshold above which days are considered days with "high radiation" (cf. Fig. 2). Concretely, we checked two other thresholds, 50 W m^{-2} and 150 W m^{-2}, for whom all source type contributions were calculated again.

Table 2
Absolute and relative contributions (in brackets) of NPF with regard to the annual average of $N_{[5-100]}$, $N_{[20-100]}$ and $N_{[5-20]}$ at Leipzig-TROPOS in 2012. The data refer to the three sub-types of method A illustrated in Fig. 6.

Variant of method A	$N_{[5-100]}$	$N_{[20-100]}$	$N_{[5-20]}$
Type 1 (original)	1.05×10^3 (14.0%)	2.83×10^2 (7.00%)	8.22×10^2 (23.8%)
Type 2 (extended into the concentration minimum on the next day)	1.14×10^3 (15.2%)	3.71×10^2 (9.17%)	8.33×10^2 (24.0%)
Type 3 (shortened to the evening rush hour, i.e., 18:00)	9.88×10^2 (13.2%)	2.35×10^2 (5.81%)	7.96×10^2 (23.1%)

The results were that the source type contributions of N_{LT} were practically insensitive (<0.1% deviation), N_{RB} weakly sensitive (0.0–3.6%) and $N_{AT\&OS}$ moderately sensitive (0.2–6.7%) towards changes in the radiation threshold. The greatest sensitivity turned out to be N_{NPF} at the urban background site L-TROPOS with regard to a radiation threshold of 50 W m^{-2}, resulting in decreases of 11% for $N_{[5-20]}$, and 21% for $N_{[20-100]}$. The apparent reason for this decrease is that the threshold of 50 W m^{-2} tends to mix days with higher particle concentrations during daytime (green dashed line in Fig. 3) into the "baseline" that is subtracted from the average cycle of $N_{\text{L-TROPOS}}$ on NPF events. For the threshold of 150 W m^{-2} any changes were 5% at maximum. The absence of a noticeable change towards a higher threshold implies that the given threshold of 100 W m^{-2} is appropriate for the intended purpose.

It can been seen in Fig. 3 that the average N on NPF event days are higher than that on non-NPF days, especially $N_{[20-100]}$. This is likely caused by the remaining newly formed particles, but meanwhile, additional particles from the traffic rush hour might interfere with the signal caused by NPF. Fig. 7 compares the average diurnal pattern of the mass concentration of black carbon (BC) and $N_{[20-100]}$ for NPF and non-NPF days. The BC mass concentration, although including particles up to 10 μm, is considered to be influenced by the traffic emissions around the site. On days without NPF event, the diurnal cycles of BC and $N_{[20-100]}$ show a distinct overall correlation throughout the day. It should be noted that the BC mass concentration is slightly lower on NPF days than on non-NPF days. If we assume that there is a positive correlation between traffic-emitted particles and BC mass concentration, we can expect that the influence of traffic-emitted particles is lower on NPF days than on non-NPF days. Therefore, by subtracting the average N on non-NPF days from that on NPF days, method B probably underestimates the contribution of NPF, rather than overestimates it.

Based on the evaluation in this section, it appears reasonable to assume that the source type contributions derived from method B are inflicted with less uncertainty than those derived by method A, particularly regarding the term N_{NPF}. However, applying of method B requires a certain amount of measurement data (several months, according to our best guess) to provide meaningful statistical average cycles such as illustrated in Fig. 3. The method is currently not able to provide source type contributions on a daily or monthly basis. Method A, in contrast, may be applied to data from individual days and can, thus, provide such results. In view of the uncertainty discussion, method A tends to provide a lower estimate for the real N_{NPF}.

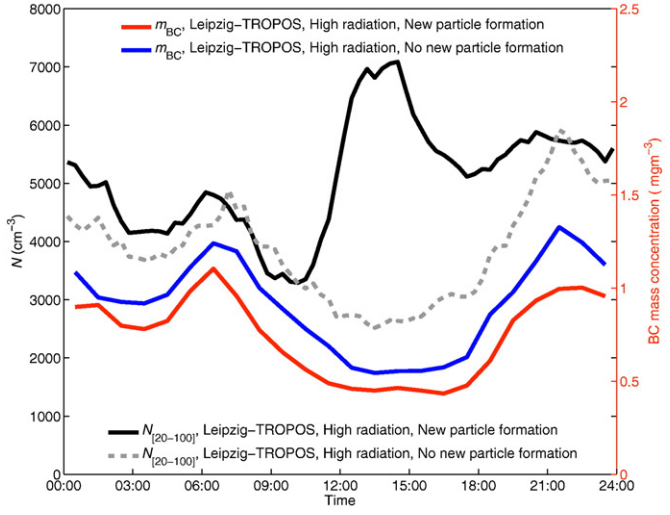

Fig. 7. Mean diurnal cycles for black carbon (BC) mass concentration and $N_{[20-100]}$ at Leipzig-TROPOS.

5. Conclusions

We estimated the contribution of photochemical particle formation to the atmospheric number concentration of ultrafine particle (UFP) in an urban atmosphere. In a first step, photochemical particle formation events were identified by the occurrence of high concentrations of small particles (<20 nm) around mid-day, and the subsequent dynamic growth of these particles into larger diameters. The contributions of new particle formation (NPF) events to the annual and monthly mean concentrations were then calculated by extracting the visible peak in the time series of UFP concentrations at the regional and urban background sites, and by assuming spatial homogeneity of the NPF event within the city, i.e., including the roadside site featuring a local concentration increment due to motor traffic. Two different methods were used that are based on different assumptions regarding the evolution of the diurnal cycle of UFPs in the absence of a NPF event. Except for the source contributions with respect to the parameter $N_{[20-100]}$ (where differences in annual mean contributions could amount up to 20%) the two methods including their variants showed only modest deviations.

Overall, the relative contribution of NPF events on $N_{[5-100]}$ average turned out to be 7% for roadside, 14% for the urban background location, and 30% at the regional background site. Their relative contribution with respect to $N_{[5-20]}$ was about twice as much due to the prevalence of newly formed particles in the lowermost size range. On individual days, the contribution of NPF events could rise up to 46% for $N_{[5-100]}$ and 95% for $N_{[5-20]}$. An evaluation on a monthly basis revealed that in Leipzig, the contribution of NPF events to UFP number concentrates on the months March-October. From November to February, NPF events played no significant role for UFP concentrations. The relative contribution of local traffic emissions at roadside was around 50%, with little sensitivity to the particular particle metric, and season.

This paper illustrates a straightforward way to differentiate available atmospheric exposure data of UFPs into different source types. While many researchers have pointed out the great importance of NPF events on urban UFP exposures on individual days, a critical assessment with respect to long-term averages has, to our knowledge, been lacking. We expect these results to contribute to a more differentiated view towards environmental UFPs in the context of growing experimental data bases that will supply environmental health studies in the future.

Acknowledgments

We acknowledge funding by the German Federal Environment Ministry (BMU) grants F&E 370343200 and F&E 371143232, supervised by Klaus Wirtz, UBA Langen. We are highly grateful to Fabian Rasch and Thomas M. Tuch for collecting and processing most of the data used in this work. André Sonntag assisted in data processing, Maik Merkel and Kay Weinhold in quality assurance experiments. We thank Gunter

Löschau (Saxon State Office for Environment, Agriculture and Geology) and Alfred Wiedensohler for the discussions within the framework of the Leipzig Low Emission Zone measurements. Horst-G. Kath (State Dept. for Environmental and Agricultural Operations in Saxony) gave permission to conduct measurements in Leipzig-Mitte. Finally, we thank three anonymous reviewers who considerably helped improve the manuscript.

Appendix A

In the regional background site Melpitz, the daily average number concentration of regional back ground aerosol ($\overline{N}_{RBG}$) and newly formed aerosol ($\overline{N}_{NPF}$) for certain size ranges can be calculated as follows:

$$\overline{N}_{RBG} = \frac{\int_0^{t_{beg}} N_{Melpitz} \cdot dt + \int_{t_{end}}^{24} N_{Melpitz} \cdot dt + \frac{1}{2}\left(N_{beg} + N_{end}\right) \cdot \left(t_{end} - t_{beg}\right)}{24} \tag{A1}$$

$$\overline{N}_{NPF} = \frac{\int_0^{24} N_{Melpitz} \cdot dt}{24} - \overline{N}_{RBG} \tag{A2}$$

where, t_{beg} and t_{end} are respectively the start and end time of the new particle formation event. $N_{Melpitz}$ is the number concentration measured in Melpitz. N_{beg} and N_{end} are respectively the back ground number concentration before and after new particle formation events.

Similar to Melpitz, the daily average number concentration of urban background aerosol ($\overline{N}_{UBG}$) and newly formed aerosol ($\overline{N}_{NPF}$) for certain size ranges in Leipzig was estimated as follows:

$$\overline{N}_{UBG} = \frac{\int_0^{t_{beg}} N_{L-TROPOS} \cdot dt + \int_{t_{end}}^{24} N_{L-TROPOS} \cdot dt + \frac{1}{2}\left(N_{beg} + N_{end}\right) \cdot \left(t_{end} - t_{beg}\right)}{24} \tag{A3}$$

$$\overline{N}_{NPF} = \frac{\int_0^{24} N_{L-TROPOS} \cdot dt}{24} - \overline{N}_{UBG} \tag{A4}$$

where, t_{beg} and t_{end} are respectively the start and end time of the new particle formation event. $N_{L\ -\ TROPOS}$ is the number concentration measured at urban background site (Leipzig-TROPOS). N_{beg} and N_{end} are the number concentrations at the urban background site before and after new particle formation events.

The contribution of local traffic to the concentration measured at roadside was estimated as follows:

$$\overline{N}_{LT} = \frac{\int_0^{24} N_{L-Mitte} \cdot dt}{24} - \overline{N}_{UBG} - \overline{N}_{NPF} \tag{A5}$$

where, $N_{L\ -\ Mitte}$ is the number concentration measured at roadside (Leipzig-Mitte). And the contribution of aged traffic/other urban sources aerosol was estimated as:

$$\overline{N}_{AT\&OS} = \overline{N}_{UBG} - \overline{N}_{RBG}. \tag{A6}$$

Appendix B

In method B, the contributions of different sources are estimated based on the average diurnal pattern of N in a set of days regarding the occurrence of new particle formation event and the global radiation level.

In Leipzig, the average number concentrations of regional background particles for high radiation days and low radiation days are respectively calculated as:

$$\overline{N}_{RBG-HR} = \frac{\int_0^{24} \widetilde{N}_{Melpitz-HR-NON} \cdot dt}{24} \tag{B1}$$

$$\overline{N}_{RBG-LR} = \frac{\int_0^{24} \widetilde{N}_{Melpitz-LR-NON} \cdot dt}{24} \tag{B2}$$

where, $\tilde{N}$ is the average diurnal variation of measured number concentration in a set of selected days. The subscript of $\tilde{N}$ denotes the station of the measurement (Melpitz/L-TROPOS/L-Mitte), the radiation level (HR/LR) and the occurrence of new particle formation event (NPF/NON). The same rules will be used also in the following equations and will not be described again. The average number concentrations of aged traffic/other urban sources particles for high radiation days and low radiation days are respectively calculated as:

$$\overline{N}_{AT\&OS-HR} = \frac{\int_0^{24} \left(\widetilde{N}_{L-TROPOS-HR-NON} - \widetilde{N}_{Melpitz-HR-NON}\right) \cdot dt}{24} \tag{B3}$$

$$\overline{N}_{AT\&OS-LR} = \frac{\int_0^{24} \left(\widetilde{N}_{L-TROPOS-LR-NON} - \widetilde{N}_{Melpitz-LR-NON}\right) \cdot dt}{24}. \tag{B4}$$

The average number concentrations of newly formed particles for high radiation days and low radiation days are respectively calculated as:

$$\overline{N}_{NPF-HR} = \frac{\int_0^{24} \left(\widetilde{N}_{L-TROPOS-HR-NPF} - \widetilde{N}_{L-TROPOS-HR-NON}\right) \cdot dt}{24} \tag{B5}$$

$$\overline{N}_{NPF-LR} = \frac{\int_0^{24} \left(\widetilde{N}_{L-TROPOS-LR-NPF} - \widetilde{N}_{L-TROPOS-LR-NON}\right) \cdot dt}{24}. \tag{B6}$$

The average number concentrations of local traffic-emitted particles for high/low radiation days and NPF/non-NPF days are respectively calculated as:

$$\overline{N}_{LT-HR-NPF} = \frac{\int_0^{24} \left(\widetilde{N}_{L-Mitte-HR-NPF} - \widetilde{N}_{L-TROPOS-HR-NPF}\right) \cdot dt}{24} \tag{B7}$$

$$\overline{N}_{LT-HR-NON} = \frac{\int_0^{24} \left(\widetilde{N}_{L-Mitte-HR-NON} - \widetilde{N}_{L-TROPOS-HR-NON}\right) \cdot dt}{24} \tag{B8}$$

$$\overline{N}_{LT-LR-NPF} = \frac{\int_0^{24} \left(\widetilde{N}_{L-Mitte-LR-NPF} - \widetilde{N}_{L-TROPOS-LR-NPF}\right) \cdot dt}{24} \tag{B9}$$

$$\overline{N}_{LT-LR-NON} = \frac{\int_0^{24} \left(\widetilde{N}_{L-Mitte-LR-NON} - \widetilde{N}_{L-TROPOS-LR-NON}\right) \cdot dt}{24}. \tag{B10}$$

Assuming the number of days with high/low radiation and NPF/non-NPF are respectively $n_{HR\ -\ NPF}$, $n_{HR\ -\ NON}$, $n_{LR\ -\ NPF}$ and $n_{LR\ -\ NON}$, the overall contribution of different sources can be calculated as follows:

$$\overline{N}_{RBG} = \frac{\overline{N}_{RBG-HR} \cdot \left(n_{HR-NPF} + n_{HR-NON}\right) + \overline{N}_{RBG-LR} \cdot \left(n_{LR-NPF} + n_{LR-NON}\right)}{n_{HR-NPF} + n_{HR-NON} + n_{LR-NPF} + n_{LR-NON}} \tag{B11}$$

$$\overline{N}_{AT\&OS} = \frac{\overline{N}_{AT\&OS-HR} \cdot (n_{HR-NPF} + n_{HR-NON}) + \overline{N}_{AT\&OS-LR} \cdot (n_{LR-NPF} + n_{LR-NON})}{n_{HR-NPF} + n_{HR-NON} + n_{LR-NPF} + n_{LR-NON}} \tag{B12}$$

$$\overline{N}_{NPF} = \frac{\overline{N}_{NPF-HR} \cdot n_{HR-NPF} + \overline{N}_{NPF-LR} \cdot n_{LR-NPF}}{n_{HR-NPF} + n_{HR-NON} + n_{LR-NPF} + n_{LR-NON}} \tag{B13}$$

$$\overline{N}_{LT} = \frac{\overline{N}_{LT-HR-NPF} \cdot n_{HR-NPF} + \overline{N}_{LT-HR-NON} \cdot n_{HR-NON}}{n_{HR-NPF} + n_{HR-NON} + n_{LR-NPF} + n_{LR-NON}} + \tag{B14}$$

$$= \frac{\overline{N}_{LT-LR-NPF} \cdot n_{LR-NPF} + \overline{N}_{LT-LR-NON} \cdot n_{LR-NON}}{n_{HR-NPF} + n_{HR-NON} + n_{LR-NPF} + n_{LR-NON}}.$$

In Melpitz, the average number concentrations of regional background particles for high radiation days and low radiation days can be respectively calculated as Eqs. (B1) and (B2). The average number concentrations of newly formed particles for high radiation days and low radiation days are respectively calculated as:

$$\overline{N}_{NPF-HR} = \frac{\int_0^{24} \left(\widetilde{N}_{Melpitz-HR-NPF} - \widetilde{N}_{Melpitz-HR-NON}\right) \cdot dt}{24} \tag{B15}$$

$$\overline{N}_{NPF-LR} = \frac{\int_0^{24} \left(\widetilde{N}_{Melpitz-LR-NPF} - \widetilde{N}_{Melpitz-LR-NON}\right) \cdot dt}{24}. \tag{B16}$$

The overall contribution of regional background aerosol and newly formed aerosol can be calculated as follows:

$$\overline{N}_{RBG} = \frac{\overline{N}_{RBG-HR} \cdot (n_{HR-NPF} + n_{HR-NON}) + \overline{N}_{RBG-LR} \cdot (n_{LR-NPF} + n_{LR-NON})}{n_{HR-NPF} + n_{HR-NON} + n_{LR-NPF} + n_{LR-NON}} \tag{B17}$$

$$\overline{N}_{NPF} = \frac{\overline{N}_{NPF-HR} \cdot n_{HR-NPF} + \overline{N}_{NPF-LR} \cdot n_{LR-NPF}}{n_{HR-NPF} + n_{HR-NON} + n_{LR-NPF} + n_{LR-NON}}. \tag{B18}$$

References

Allan, J.D., Alfarra, M.R., Bower, K.N., Coe, H., Jayne, J.T., Worsnop, D.R., et al., 2006. Size and composition measurements of background aerosol and new particle growth in a Finnish forest during QUEST 2 using an Aerodyne Aerosol Mass Spectrometer. Atmos. Chem. Phys. 6, 315–327.

Asmi, A., Wiedensohler, A., Laj, P., Fjaeraa, A.M., Sellegri, K., Birmili, W., et al., 2011. Number size distributions and seasonality of submicron particles in Europe 2008–2009. Atmos. Chem. Phys. 11 (11), 5505–5538.

Birmili, W., Stratmann, F., Wiedensohler, A., 1999. Design of a DMA-based size spectrometer for a large particle size range and stable operation. J. Aerosol Sci. 30 (4), 549–553.

Birmili, W., Berresheim, H., Plass-Dülmer, C., Elste, T., Gilge, S., Wiedensohler, A., et al., 2003. The Hohenpeissenberg aerosol formation experiment (HAFEX): a long-term study including size-resolved aerosol, H_2SO_4, OH, and monoterpenes measurements. Atmos. Chem. Phys. 3, 361–376.

Birmili, W., Alaviippola, B., Hinneburg, D., Knoth, O., Tuch, T., Borken-Kleefeld, J., et al., 2009a. Dispersion of traffic-related exhaust particles near the Berlin urban motorway — estimation of fleet emission factors. Atmos. Chem. Phys. 9 (7), 2355–2374.

Birmili, W., Weinhold, K., Nordmann, S., Wiedensohler, A., Spindler, G., Mueller, K., et al., 2009b. Atmospheric aerosol measurements in the German Ultrafine Aerosol Network (GUAN). Gefahrstoffe Reinhalt. Luft 69 (4), 137–145.

Birmili, W., Tomsche, L., Sonntag, A., Opelt, C., Weinhold, K., Nordmann, S., et al., 2013. Variability of aerosol particles in the urban atmosphere of Dresden (Germany): effects of spatial scale and particle size. Meteorol. Z. 22 (2), 195–211.

Boy, M., Kulmala, M., 2002. Nucleation events in the continental boundary layer: Influence of physical and meteorological parameters. Atmos. Chem. Phys. 2, 1–16.

Costabile, F., Birmili, W., Klose, S., Tuch, T., Wehner, B., Wiedensohler, A., et al., 2009. Spatio-temporal variability and principal components of the particle number size distribution in an urban atmosphere. Atmos. Chem. Phys. 9 (9), 3163–3195.

Dal Maso, M., Kulmala, M., Riipinen, I., Wagner, R., Hussein, T., Aalto, P.P., et al., 2005. Formation and growth of fresh atmospheric aerosols: eight years of aerosol size distribution data from SMEAR II, Hyytiala, Finland. Boreal Environ. Res. 10 (5), 323–336.

Dall'Osto, M., Querol, X., Alastuey, A., O'Dowd, C., Harrison, R.M., Wenger, J., Gómez-Moreno, F.J., 2013. On the spatial distribution and evolution of ultrafine particles in Barcelona. Atmos. Chem. Phys. 13, 741–759.

Engler, C., Birmili, W., Spindler, G., Wiedensohler, A., 2012. Analysis of exceedances in the daily PM_{10} mass concentration (50 μg m^{-3}) at a roadside station in Leipzig, Germany. Atmos. Chem. Phys. 12 (21), 10107–10123.

Franck, U., Odeh, S., Wiedensohler, A., Wehner, B., Herbarth, O., 2011. The effect of particle size on cardiovascular disorders — the smaller the worse. Sci. Total Environ. 409 (20), 4217–4221.

Giechaskiel, B., Ntziachristos, L., Samaras, Z., Scheer, V., Casati, R., Vogt, R., 2005. Formation potential of vehicle exhaust nucleation mode particles on-road and in the laboratory. Atmos. Environ. 39 (18), 3191–3198.

Graham, L., 2005. Chemical characterization of emissions from advanced technology light-duty vehicles. Atmos. Environ. 39 (13), 2385–2398.

Grose, M., Sakurai, H., Savstrom, J., Stolzenburg, M.R., Watts, W.F., Morgan, C.G., et al., 2006. Chemical and physical properties of ultrafine diesel exhaust particles sampled downstream of a catalytic trap. Environ. Sci. Technol. 40 (17), 5502–5507.

Hamed, A., Birmili, W., Joutsensaari, J., Mikkonen, S., Asmi, A., Wehner, B., et al., 2010. Changes in the production rate of secondary aerosol particles in Central Europe in view of decreasing SO_2 emissions between 1996 and 2006. Atmos. Chem. Phys. 10 (3), 1071–1091.

Harris, S.J., Maricq, M.M., 2001. Signature size distributions for diesel and gasoline engine exhaust particulate matter. J. Aerosol Sci. 32 (6), 749–764.

HEI Review Panel on Ultrafine Particles, 2013. Understanding the Health Effects of Ambient Ultrafine Particles. HEI Perspectives 3. Health Effects Institute, Boston, MA.

Heintzenberg, J., Wehner, B., Birmili, W., 2007. 'How to find bananas in the atmospheric aerosol': new approach for analyzing atmospheric nucleation and growth events. Tellus Ser. B Chem. Phys. Meteorol. 59 (2), 273–282.

Kittelson, D.B., 1998. Engines and nanoparticles: a review. J. Aerosol Sci. 29 (5–6), 575–588.

Kulmala, M., Vehkamäki, H., Petäjä, T., Dal Maso, M., Lauri, A., Kerminen, V.M., et al., 2004. Formation and growth rates of ultrafine atmospheric particles: a review of observations. J. Aerosol Sci. 35 (2), 143–176.

Kumar, P., Morawska, L., Birmili, W., Paasonen, P., Hu, M., Kulmala, M., et al., 2014. Ultrafine particles in cities. Environ. Int. 66, 1–10.

Lenschow, P., Abraham, H.J., Kutzner, K., Lutz, M., Preuss, J.D., Reichenbacher, W., 2001. Some ideas about the sources of PM_{10}. Atmos. Environ. 35, S23–S33.

Manninen, H.E., Nieminen, T., Asmi, E., Gagne, S., Hakkinen, S., Lehtipalo, K., et al., 2010. EUCAARI ion spectrometer measurements at 12 European sites — analysis of new particle formation events. Atmos. Chem. Phys. 10 (16), 7907–7927.

Maricq, M.M., 2007. Chemical characterization of particulate emissions from diesel engines: a review. J. Aerosol Sci. 38 (11), 1079–1118.

Morawska, L., Ristovski, Z., Jayaratne, E.R., Keogh, D.U., Ling, X., 2008. Ambient nano and ultrafine particles from motor vehicle emissions: characteristics, ambient processing and implications on human exposure. Atmos. Environ. 42 (35), 8113–8138.

Ntziachristos, L., Mamakos, A., Samaras, Z., et al., 2004. Overview of the European Particulates project on the characterization of exhaust particulate emissions from road vehicles: results for light-duty vehicles. SAE Trans. 113 (4), 1354–1373.

Peters, A., Wichmann, H.E., Tuch, T., Heinrich, J., Heyder, J., 1997. Respiratory effects are associated with the number of ultrafine particles. Am. J. Respir. Crit. Care Med. 155 (4), 1376–1383.

Pfeifer, S., Birmili, W., Schladitz, A., Müller, T., Nowak, A., Wiedensohler, A., 2014. A fast and easy-to-implement inversion algorithm for mobility particle size spectrometers considering particle number size distribution information outside of the detection range. Atmos. Meas. Tech. 7 (1), 95–105.

Rasch, F., Birmili, W., Weinhold, K., Nordmann, S., Sonntag, A., Spindler, G., et al., 2013. Significant reduction of ambient black carbon and particle number in Leipzig as a result of the low emission zone. Gefahrstoffe Reinhalt. Luft 73 (11–12), 483–489.

Riccobono, F., Schobesberger, S., Scott, C.E., Dommen, J., Ortega, I.K., Rondo, L., et al., 2014. Oxidation products of biogenic emissions contribute to nucleation of atmospheric particles. Science 344, 717–721.

Rückerl, R., Schneider, A., Breitner, S., Cyrys, J., Peters, A., 2011. Health effects of particulate air pollution: a review of epidemiological evidence. Inhal. Toxicol. 23 (10), 555–592.

Sakurai, H., Tobias, H.J., Park, K., Zarling, D., Docherty, K.S., Kittelson, D.B., et al., 2003. On-line measurements of diesel nanoparticle composition and volatility. Atmos. Environ. 37 (9–10), 1199–1210.

Shen, X.J., Sun, J.Y., Zhang, Y.M., Wehner, B., Nowak, A., Tuch, T., et al., 2011. First long-term study of particle number size distributions and new particle formation events of regional aerosol in the North China Plain. Atmos. Chem. Phys. 11 (4), 1565–1580.

Sipilä, M., Berndt, T., Petäjä, T., Brus, D., Vanhanen, J., Stratmann, F., et al., 2010. The role of sulfuric acid in atmospheric nucleation. Science 327 (5970), 1243–1246.

Smith, J.N., Moore, K.F., Eisele, F.L., Voisin, D., Ghimire, A.K., Sakurai, H., et al., 2005. Chemical composition of atmospheric nanoparticles during nucleation events in Atlanta. J. Geophys. Res.-Atmos. 110 (D22), 13.

Smith, J.N., Dunn, M.J., VanReken, T.M., Iida, K., Stolzenburg, M.R., McMurry, P.H., et al., 2008. Chemical composition of atmospheric nanoparticles formed from nucleation in Tecamac, Mexico: evidence for an important role for organic species in nanoparticle growth. Geophys. Res. Lett. 35 (4), 5.

Tobias, H.J., Beving, D.E., Ziemann, P.J., Sakurai, H., Zuk, M., McMurry, P.H., et al., 2001. Chemical analysis of diesel engine nanoparticles using a nano-DMA/thermal desorption particle beam mass spectrometer. Environ. Sci. Technol. 35 (11), 2233–2243.

Vana, M., Kulmala, M., Dal Maso, M., Horrak, U., Tamm, E., 2004. Comparative study of nucleation mode aerosol particles and intermediate air ions formation events at three sites. J. Geophys. Res.-Atmos. 109 (D17), 10.

Wehner, B., Siebert, H., Stratmann, F., Tuch, T., Wiedensohler, A., Petaja, T., et al., 2007. Horizontal homogeneity and vertical extent of new particle formation events. Tellus Ser. B Chem. Phys. Meteorol. 59 (3), 362–371.

WHO, 2013. Review of Evidence on Health Aspects of Air Pollution—REVIHAAP Project: Final Technical Report.

Wiedensohler, A., Birmili, W., Nowak, A., Sonntag, A., Weinhold, K., Merkel, M., et al., 2012. Mobility particle size spectrometers: harmonization of technical standards and data structure to facilitate high quality long-term observations of atmospheric particle number size distributions. Atmos. Meas. Tech. 5 (3), 657–685.

Zhu, Y.F., Hinds, W.C., Kim, S., Sioutas, C., 2002. Concentration and size distribution of ultrafine particles near a major highway. J. Air Waste Manage. Assoc. 52 (9), 1032–1042.

Zwack, L.M., Hanna, S.R., Spengler, J.D., Levy, J.I., 2011. Using advanced dispersion models and mobile monitoring to characterize spatial patterns of ultrafine particles in an urban area. Atmos. Environ. 45 (28), 4822–4829.